Available online at www.sciencedirect.com
ScienceDirect
Electrochimica Acta 52 (2007) 6929–6937
ELECTROCHIMICA Acta
www.elsevier.com/locate/electacta

Participation of the dissolved O_2 in the passive layer formation on Zn surface in neutral media

Hamdy H. Hassan [a,*], Mohammed A. Amin [a], S. Gubbala [b], M.K. Sunkara [b]

[a] *Chemistry Department, Faculty of Science, Ain Shams University, Cairo 11566, Egypt*
[b] *Department of Chemical Engineering, University of Louisville, Louisville, KY 40292, USA*

Received 19 March 2007; received in revised form 5 May 2007; accepted 6 May 2007
Available online 13 May 2007

Abstract

The composition of the passive layers formed on Zn electrode in naturally aerated and de-aerated 0.1 M $KClO_4$ solution were studied using X-ray photoelectron spectroscopic measurements (XPS). A correlation between the presence of dissolved O_2 and the formation of an interior passive layer was carried out. Librated Cl^- from the perchlorate reduction reaction was detected in its solutions during Zn electrode polarization. The librated Cl^- concentration reached its maximum value at −1.4 V. Moreover, in the studied potential range the perchlorate reduction rate increases in absence of dissolved oxygen. Chrono-amperometry and electrochemical impedance spectroscopy (EIS) were performed for the stationary and the rotating disc Zn electrodes in naturally aerated and de-aerated 0.1 M $KClO_4$ solution. EIS technique showed a change in the electrode impedance with the experimental conditions as a result of changing the reactions occurring in the electrode vicinity. The obtained data were fitted to three different equivalent circuits depending on the electrode potential. The protective nature of the passive layers formed in different experimental conditions was found to decrease with rotating the electrode and de-aerating the solution.

Keywords: XPS; EIS; Perchlorate reduction; Oxygen reduction; Passive layer

1. Introduction

There has been a great deal of interest in the electrochemical behaviour of Zn electrode and the various processes taking place during its corrosion in various neutral media [1–11]. Most of these reports agreed that Zn corrosion process in neutral media is limited by a diffusion controlled oxygen reduction reaction. The recent work of Láng et al. [12–15] demonstrates the reduction of ClO_4^- ions on a variety of metal surfaces, to Cl^- and OH^-, during their spontaneous dissolution. Such reduction during the Zn corrosion represents an alternative source of OH^- production. Our recent study of the voltammetric behaviour of Zn in perchlorate solutions [1,2] offers some mechanistic information about the passive layer formation in neutral media. This work emphasized the necessity of the presence of dissolved oxygen, and not merely the OH^-, to form a more protective passive layer. Moreover, the passive layers formed on the Zn surface in neutral media were suggested to be composed of interior compact ZnO layer and an exterior porous $Zn(OH)_2$/ZnO layer. The presence of O_2 was found to be a must to form a thicker more protective interior layer [1]. Moreover, the cathodic peaks of the interior passive layers reduction were vanished from the voltammograms obtained in de-aerated perchlorate solutions. These results encourage us to study the chrono-amperometric and the impedance responses of the Zn/perchlorate interphase under the influence of different experimental conditions with the aim to confirm, and add more knoweldge to, our previously obtained results [1,2].

2. Experimental

All electrolyte solutions were prepared from analytical grade chemicals and doubly distilled water. The de-aerated solutions were sparged with N_2 gas for 30 min prior to use. N_2 bubbling was stopped and nitrogen blanket was maintained over the solution throughout the experiment.

The working electrode was a Zn disc (99.9999% Koch Light Laboratories, Colnbrook Bucks, England) with an apparent

* Corresponding author.
E-mail addresses: hamdihh@hotmail.com, hamdihh@yahoo.com (H.H. Hassan).

0013-4686/$ – see front matter © 2007 Elsevier Ltd. All rights reserved.
doi:10.1016/j.electacta.2007.05.013

exposed area of 0.5 cm^2. It was inserted in a rotating disc system developed by Solea-Tacussel. The electrode was successively polished with emery papers of 600 and 1000 grit sizes, degreased with acetone and washed with running doubly distilled water. The counter electrode was a platinum sheet (4 cm^2). The potentials were recorded versus a saturated silver–silver chloride electrode (Ag/AgCl). To avoid contamination, the reference electrode was connected to the working electrode through a bridge filled with the solution under test. Each experiment was performed with freshly prepared solutions and a newly polished set of electrodes. All measurements were carried out at $25 \pm 1\,^{\circ}C$.

Chrono-amperometric curves, at different electrode potentials, were recorded for 400 s. EIS measurements were carried out using AC signals of amplitude 5 mV peak to peak at different conditions in the frequency range of 10 kHz to 10 mHz. An Autolab Potentiostat/Galvanostat (PGSTAT30) with FRA2 module was used for these measurements.

Detection of the librated Cl^- from the perchlorate reduction during the polarization of the Zn electrode was performed as follows: the potential of the stationary Zn was hold to the desired potential values for 3 h in 30 ml of a continuously stirred 0.5 M $NaClO_4$ solution. Afterwards, chloride concentration was measured potentiometrically in this solution using an Ag/AgCl selective electrode (detection limit: 200 ppm Cl^-) and a HANNA pH-meter model pH211.

X-ray photoelectron spectroscopic measurements (XPS) were performed using a VG Scientific X-ray photoelectron spectrometer with an XR3E2 X-ray source system. The instrument error is ±0.4 eV. The XPS spectra for Zn $2p_{3/2}$ and O 1s were recoded for the surface of the zinc electrode that is polarized from −1.8 to −1.15 V with a scan rate of 1.0 mV s^{-1} and hold at −1.15 V for 20 min in naturally aerated and de-aerated 0.1 M $KClO_4$ solutions.

3. Results and discussion

3.1. Cyclic voltammetric studies

In a recent study [1], we divided the voltammograms of the Zn electrode in 0.1 M $KClO_4$ solution into four different potential regions, as shown in Fig. 1. The different electrochemical and chemical reactions occurred at the Zn electrode surface in different experimental conditions were discussed. In region 1, between −1.8 and −1.48 V, water reduction reaction is predominant. However, in region 2, between −1.48 and −1.32 V, the diffusion controlled oxygen reduction reaction takes place according to Eq. (1) [1,9,16,17]:

$$O_2 + 2H_2O + 4e = 4OH^- \quad (1)$$

In the third potential region, between −1.32 and −1.05 V, in addition to reaction (1), the anodic dissolution of zinc commences. On the other hand, the ClO_4^- ions in contact with Zn electrode surface reduces according to the overall reaction [1,18]:

$$ClO_4^- + 4H_2O + 8e = Cl^- + 8OH^- \quad (2)$$

The concentration of the librated chloride ion is measured, using chloride selective electrode, after holding the Zn electrode for 3 h at desired fixed potential values, the results are given in Table 1. According to these results, the quantity of chloride formed varies with the applied potential. The maximum chloride concentration was obtained in the potential range of region 2 (at −1.4 V). The amount of librated Cl^- in this potential is doubled by de-aeration (see Table 1). Although ClO_4^- reduction still occurs at potentials lower and higher than this range, chloride ion concentration decreases drastically. Similar results were previously obtained for the reduction of perchlorate on tin electrode [19].

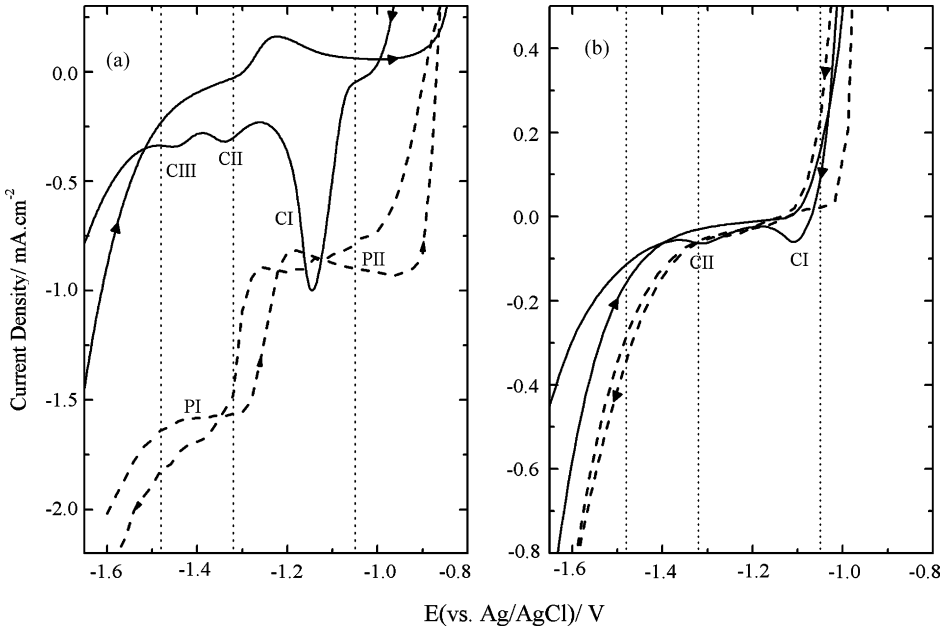

Fig. 1. Cyclic voltammograms for stationary (solid line) and 64 rad s^{-1} rotating Zn electrode (dotted lines) in naturally aerated (a) and de-aerated (b) 0.1 M $KClO_4$ at scan rate of 0.5 mV/s.

Table 1
The librated chloride concentration [Cl^-], after holding the Zn electrode for 3 h at different potential values in 30 ml of the 0.5 M $NaClO_4$ solution

E_{Zn} (vs. Ag/AgCl) (V)	[Cl^-] (ppm)	
	De-aerated solution	Naturally aerated solution
−1.800	219	209
−1.700	395	325
−1.600	UDL[a]	UDL
−1.500	231	505
−1.400	8621	1800
−1.300	584	395
−1.200	1218	504
−1.100	746	415
−1.000	UDL	480

[Cl^-] detected by the chloride selective electrode with detection limit of 200 ppm.
[a] UDL, under the detection limit.

3.2. X-ray photoelectron spectroscopy

The consecutive and parallel paths mechanism suggested for Zn dissolution in aerated [7] and de-aerated [20,21] neutral solutions, together with reactions ((1) and (2)), lead to the formation of a passive layer on the Zn surface. XPS spectra of Zn $2p_{3/2}$ and O 1s for the passive layer formed on Zn surface in the corresponding potential range are shown in Fig. 2 the passive layer was prepared by polarizing the Zn electrode from −1.8 to −1.15 V with scan rate of 1.0 mV s^{-1} in naturally aerated and de-aerated 0.1 M $KClO_4$ solutions, then the electrode potential was hold at −1.15 V for 20 min. Depicting the binding energy (BE) for O 1s and Zn $2p_{3/2}$ on XPS spectra, reveals that the passive layer is a mixture of $Zn(OH)_2$ and ZnO. According to the Zn $2p_{3/2}$ survey, a broad peak at about 1021 eV is obtained. This peak is resolved to two peaks: the first is an intense peak at a BE of about 1021.1 eV which may be seen as an overlap of Zn^0 and ZnO peaks (the reported BE values are 1021 eV for Zn^0 and 1021.2 eV for ZnO [22]); the second peak is the $Zn(OH)_2$ peak at 1023 eV (the reported BE value is 1022.7 eV [23]). From O 1s line deconvolution presented in Fig. 2b and d, oxygen appears in four chemical states. The first appears at 533.9 eV and attributed to adsorbed water molecules [24], the second and the third appear at 532.1 and 530.4 eV and are related to the formation of $Zn(OH)_2$ and ZnO, respectively [25]. The fourth appears at 529 eV and may be ascribed to chemisorbed O_2 on Zn metal; O_2/Zn. Actually, we did not find a BE value for O_2/Zn in the literature, however, a BE value of 529.8 eV is reported for O_2/Cu [26]. This peak appears intensely in the passive layer formed in the aerated conditions (sample 1) (Fig. 2b) and diminishes drastically in the de-aerated conditions (sample 2) (Fig. 2d). Moreover, the zinc survey in Fig. 2a and c does not show any Zn peak behave similarly. Consequently, the fourth O 1s peak could not related to a Zn-oxygen compound. This suggestion matches well with the existence of the cathodic peak CIII, which was attributed to reduction of the interior passive layer in the aerated conditions (Fig. 1a) and its disappearance in de-aerated conditions (Fig. 1b). Moreover, these results contest the existence of surface species that enhances the Zn corrosion protection in aerated solutions [1].

The XPS O 1s results practiced on sample 1 surface (naturally aerated conditions) indicate significant contribution of chemisorbed O_2 and ZnO in the passive layer (Table 2). However, passive layer formed on Zn in de-aerated 0.1 M $KClO_4$ solution exhibits higher ZnO contribution at the expense of chemisorbed O_2. On the other hand, we may not count for the

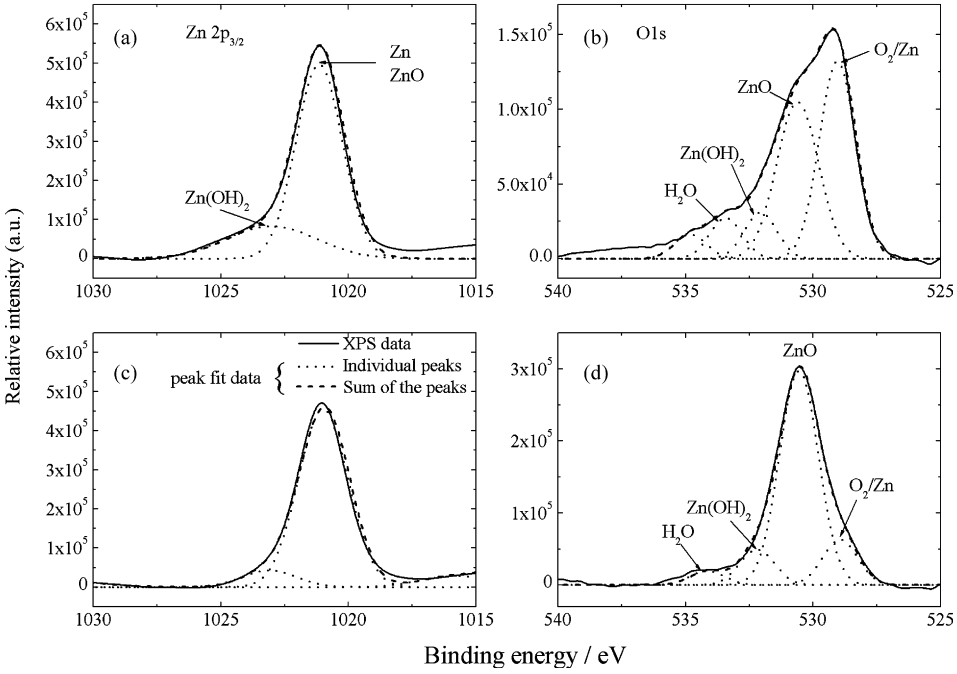

Fig. 2. XPS spectrum of Zn $2p_{3/2}$ and O Is for the film formed on zinc electrode polarized from −1.8 to −1.15 V (1 mV s^{-1}) and hold at −1.15 V for 30 min in naturally aerated (a and b) and de-aerated (c and d) 0.1 M $KClO_4$.

Table 2
Binding energies (BE) and peak area ratio (%PA) correspond to each component in the XPS spectra of Fig. 2 for the passive layers formed on Zn electrodes polarized at −1.15 V in aerated (sample 1) and de-aerated (sample 2) 0.1 M $KClO_4$ solutions

	Zn $2p_{3/2}$		O 1s			
	ZnO	$Zn(OH)_2$	O_2/Zn	ZnO	$Zn(OH)_2$	H_2O/Zn
Sample 1						
BE (eV)	1021.1	1023.0	529.0	530.6	532.1	533.4
%PA	75.2	24.8	43.1	39.9	9.0	8.0
Sample 2						
BE (eV)	1021.0	1023.1	528.9	530.6	532.2	534.1
%PA	90.7	9.3	13.6	71.6	10.7	4.2

peak area ratios derived from the Zn $2p_{3/2}$ because the peaks of Zn^0 and ZnO are very close to each other, so that the peak observed at 1021 eV may be related to their overlap.

3.3. Chrono-amperometric studies

The potentiostatic current–time transients of the stationary and rotating Zn disc electrode in naturally aerated 0.1 M $KClO_4$ solution at different electrode potentials E_a are shown in Fig. 3. In addition, Fig. 4 is its analogous in de-aerated solution. The cathodic current, in the first potential region, decreases rapidly with time till attaining a steady state value which is related to the rate of electrochemical water reduction reaction [1], curve 1 of Figs. 3 and 4. Similar behaviour is obtained in the second potential region. The higher steady state current values for the rotating electrode in naturally aerated solution is attributed to the acceleration of the slug diffusion controlled O_2 reduction reaction that predominates in aerated solutions in this potential range, curve 2 of Fig. 3a and b.

The steady state current in the third region, curves 3 and 4, composed of four superimposed partial current components, namely: charge transfer anodic metal dissolution, $j_{+,M}$, cathodic metal ion deposition (back reaction) $j_{-,M}$, diffusion controlled dissolved oxygen reduction j_{-,O_2} and ClO_4^- reduction partial current j_{-,ClO_4^-} [1,10–12]. Therefore, the total current density at a given potential is given by:

$$j_{total} = j_{+,M} + j_{-,M} + j_{-,O_2} + j_{-,ClO_4^-} \quad (3)$$

In other words, in addition to the O_2 and ClO_4^- reduction reactions, the steady state current is related to the rate of electrochemical dissolution of metal through the passive layer and chemical dissolution of this layer, so that it is a measure of the protective capabilities of the passive layer [27].

The steady state currents obtained in this potential range are all cathodic, curves (3 and 4) of Figs. 3 and 4. The steady state currents of the Zn electrode in naturally aerated solutions are always higher than their analogous in the de-aerated solutions due to the contribution of j_{-,O_2} in the former case. In naturally aerated solution, curves 3 and 4 (Fig. 3), O_2 preferentially adsorbed on the electrode surface at the expense of the weakly adsorbed ClO_4^- [13,28,29]. The steady state current of the rotating Zn electrode is higher than that of the stationary electrode as a result of enhancing j_{-,O_2} by rotation. However, in absence of oxygen, curves 3 and 4 of Fig. 4, the higher currents obtained for rotating electrode can be explained in terms of the formation of a less protective passive layer. Rotating the electrode repels the corrosion products away from the electrode surface. The perchlorate ion absorbs on the electrode surface and enhances the chemical dissolution of the interior ZnO layer to form Zn^{2+}(aq) [1,6,30]. The reduction of ClO_4^- on the electrode surface promotes the formation of the less protective exterior passive layer as a result of the high amount of OH^- produced from reaction (2).

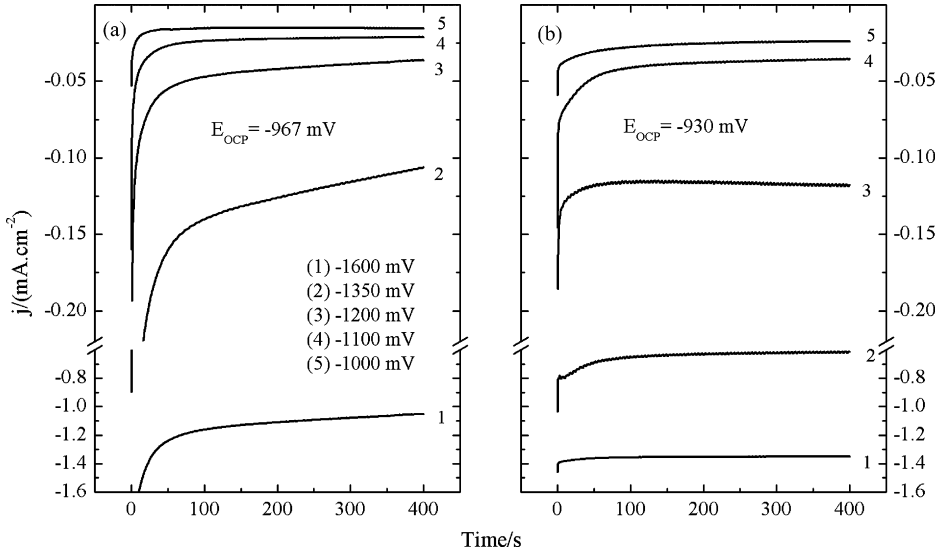

Fig. 3. Chrono-amperometric curves for stationary (a) and 64 rad s^{-1} rotating (b) Zn electrode in naturally aerated 0.1 M $KClO_4$ solution at different electrode potential.

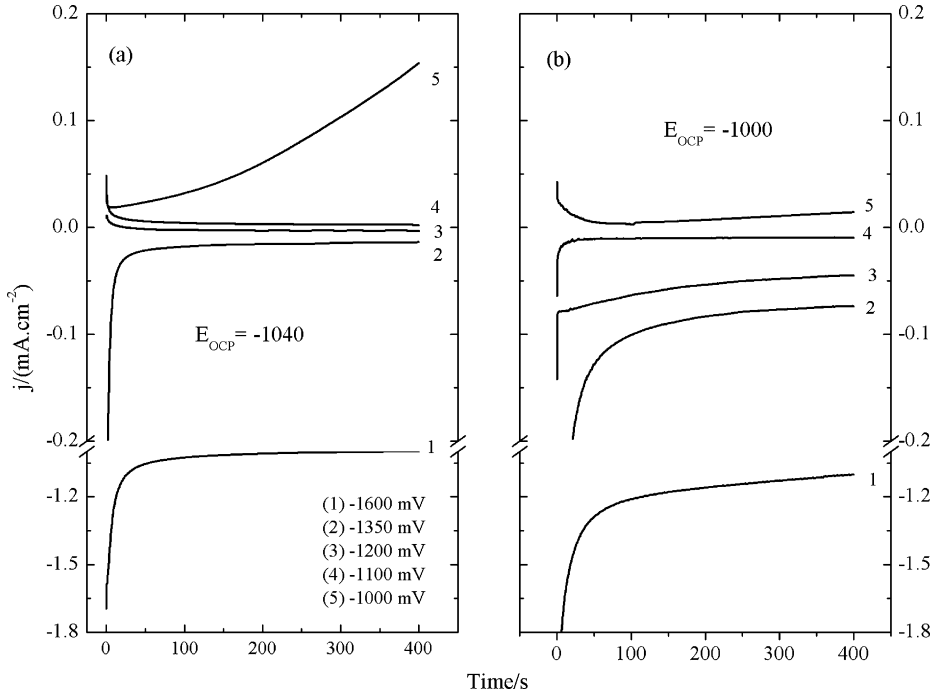

Fig. 4. Chrono-amperometric curves for stationary (a) and 64 rad s^{-1} rotating (b) Zn electrode in de-aerated 0.1 M $KClO_4$ solution at different electrode potential.

When the electrode potential moves towards more anodic potentials, at $E_s = -1000$ mV, curves 5 of Fig. 3 exhibit similar behaviour as curves 4 with lower current values. However, for de-aerated solutions the current changes to be anodic. It decreases to a minimum value and then increases tracing approximately a straight line. The increase in current density is related to the rupture of the passive layer. This behaviour occurs in the deaerated solutions at less noble potentials confirming the formation of less protective layer in this condition. Three stage chrono-amperometric curves characterizing the pitting corrosion of stationary Zn electrode in naturally aerated perchlorate solutions at more anodic potentials were previously studied [2]. The first stage involved passive layer growth while; the second and the third involved pitting nucleation and growth. The pitting nucleation rate was found to increase with increasing the applied anodic potential.

3.4. Impedance measurements

Several studies were concerned with the analysis and simulation of the impedance spectra of Zn electrodes in aerated [20,21] and deaerated [31] near neutral solutions. They agreed that the zinc surface is progressively modified when the potential values of the electrode, in contact with the aqueous solution, is increased. Fig. 5 represents the complex plane impedance and the Bode plots for the Zn disc electrode in 0.1 M $KClO_4$ solution in the first potential region (at −1.6 V) in different experimental conditions. The response of the Nyquist plane (Fig. 5a), in the frequency range 10^4–10^{-2} Hz, exhibits a high frequency capacitive loop that may be attributed to the charge-transfer water reduction reactions. The charge-transfer semicircle makes an angle approaches 90° with the real axis and their intersection gives a value of $R_o \approx 27\ \Omega$ for the resistance of the solution

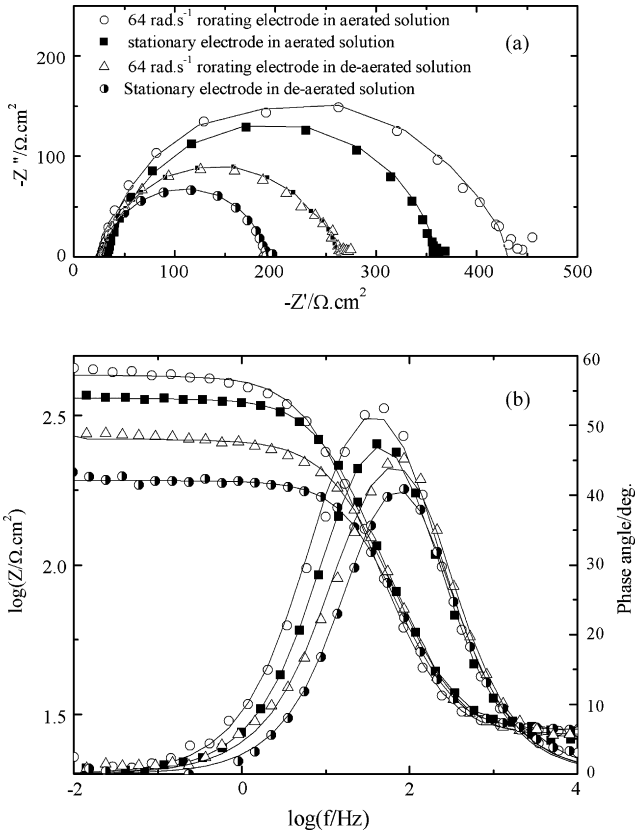

Fig. 5. Nyquist (a) and Bode (b) plots for the zinc electrode at −1.6 V in 0.1 M $KClO_4$ in the frquency range 10^4–10^{-2} Hz. Symbols represent the experimental data and solid lines represent the best fit.

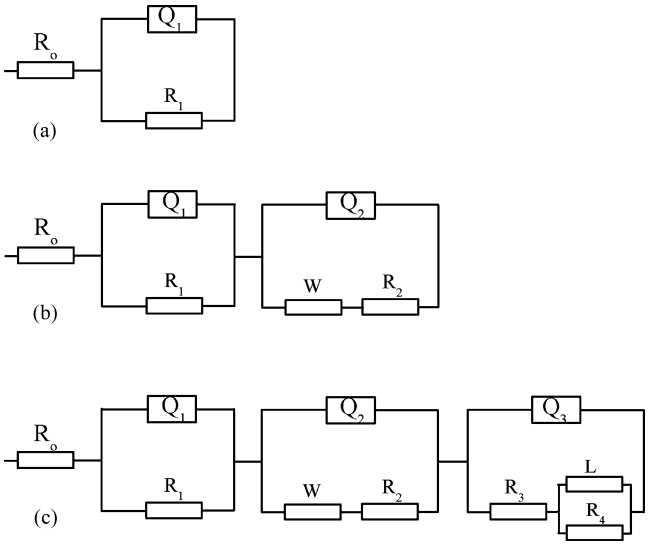

Fig. 6. The equivalent circuits used to fit the impedance data of the zinc electrode polarized at $E = -1.6$ V (a), $E = -1.35$ V (b) and $E = -1.2$ and -1.1 V (c) in 0.1 M $KClO_4$.

enclosed between the working electrode and the reference electrode. The electrode at this potential is expected to be film free [1,2]. The value of R_o does not change within the different studied experimental conditions. The intercept of the extrapolation of the charge-transfer semicircle with the real axis in the low frequency range gives a charge transfer resistance (R_1). Fig. 5b represents Bode plots recorded for the Zn electrode at -1.6 V, it provides equal representation of the impedance data and explicit appearance of the phase angle as a sensitive parameter to interfacial phenomena [32,33]. The impedance at high frequency limit ($f = 10$ kHz) corresponds to (R_o), while it corresponds to R_1 at the low frequency limit (10 mHz). This resistive behaviour is confirmed by a 0° phase angle between current and potential. At intermediate frequencies, the single maximum in the phase angle data shows the presence of only one time constant in the Bode plot [34]. Deviation of the maximum phase angles, α_{max}, from 90° and the slopes of Bode impedance magnitude plots, S, from the value of -1 accounts for the deviation from ideal capacitive behaviour. Accordingly, the obtained experimental data were fitted to the single time constant equivalent circuit of Fig. 6a. The constant phase element, CPE (Q_1), is introduced in the circuit instead of a pure double layer capacitor to account for this deviation, that may attributed to surface nonhomogeneity [35] or roughness factors [36]. The impedance of the CPE is expressed as:

$$Z_{CPE} = \frac{1}{Y_0(j\omega)^n} \quad (4)$$

where Y_0 is the magnitude of the CPE, $-1 \leq n \leq 1$. Depending on the value of n, CPE can represent pure resistance ($n = 0$), pure capacitance ($n = 1$), inductance ($n = -1$) or Warburg impedance ($n = 0.5$) [37]. The values of $0.5 \leq n \leq 1$, is related to the above mentioned non-ideal capacitive behaviour and the appearance of a depressed semicircular shape of the Nyquist plot. The electrochemical parameters obtained from the fitting process are listed in Table 3. The data of Fig. 5 and Table 3 show a shift in the characteristic frequencies of α_{max} to lower values and an increase in the values of R_1 with the electrode rotation and with the presence of dissolved O_2. This behaviour may be attributed to the decrease in the number of active sites available for the water reduction reaction. Where, with electrode rotation and in presence of dissolved O_2, the preferential adsorption of different ionic species and O_2 takes place, respectively. Moreover, the values of S and n remain almost constant.

In the second potential region, at $E = -1.35$ V, in addition to O_2 reduction, the perchlorate reduction becomes more important specially in the de-aerated solution as shown from Table 1. Bode plots at this potential show two phase angle maxima at intermediate frequencies and a continuous increase in both of the phase angle and the impedance values at low frequencies, as shown in Fig. 7. These results lead us to propose a modified two time constants equivalent circuit to fit the experimental data (Fig. 6b). The first is described above and the second of CPE (Q_2), a parallel charge-transfer resistance R_2, related to

Table 3
Impedance parameters obtained by fitting data of Fig. 5 with the equivalent circuit of Fig. 6a for the zinc electrode polarized at -1.6 V in 0.1 M $KClO_4$

Solution	Electrode	Parameter		
		$R1$ (Ω)	$Q1$	
			Y (μF cm^{-2})	n
Aerated	Stationary	328	17.7	0.87
	Rotating	404	20.1	0.86
De-aerated	Stationary	164	20.1	0.88
	Rotating	237	14.6	0.84

$R_o = 27$.

Table 4
Impedance parameters obtained by fitting data of Fig. 7 with the equivalent circuit of Fig. 6b for the zinc electrode polarized at -1.35 V in 0.1 M $KClO_4$

Solution	Electrode	Parameter						
		$R1$ (Ω)	$Q1$		$Q2$		$W \times 10^{-4}$	$R2$ (Ω)
			Y (μF cm^{-2})	n	Y (μF cm^{-2})	n		
Aerated	Stationary	1863	60.8	0.81	31.9	0.91	33.93	1521
	Rotating	3146	19.8	0.77	86.1	0.98	55.36	217
De-aerated	Stationary	1212	99.7	0.82	17.7	0.88	35.91	1272
	Rotating	980	220.3	0.93	16.5	0.86	22.37	791

$R_o = 27$.

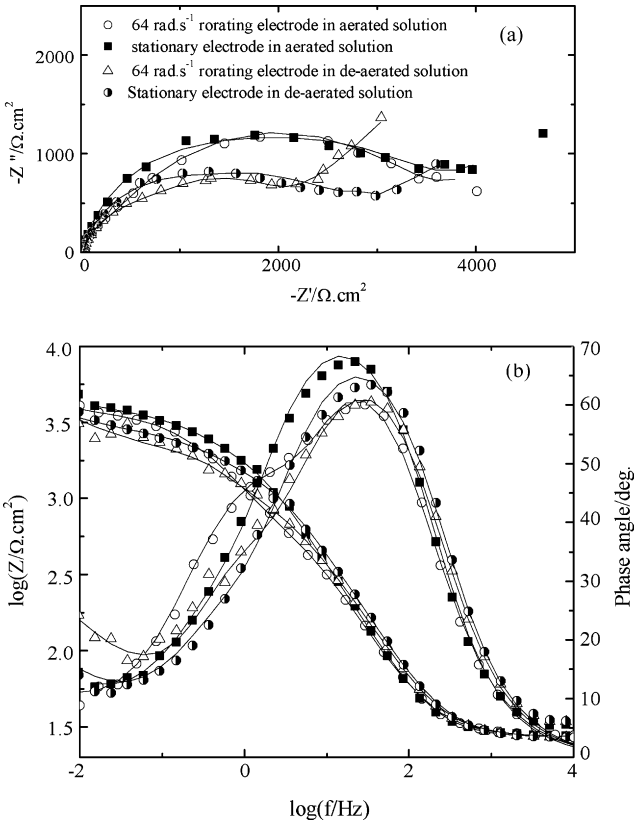

Fig. 7. Nyquist (a) and Bode (b) plots for the zinc electrode at −1350 mV in 0.1 M $KClO_4$ in the frquency range 10^4–10^{-2} Hz. Symbols represent the experimental data and solid lines represent the best fit.

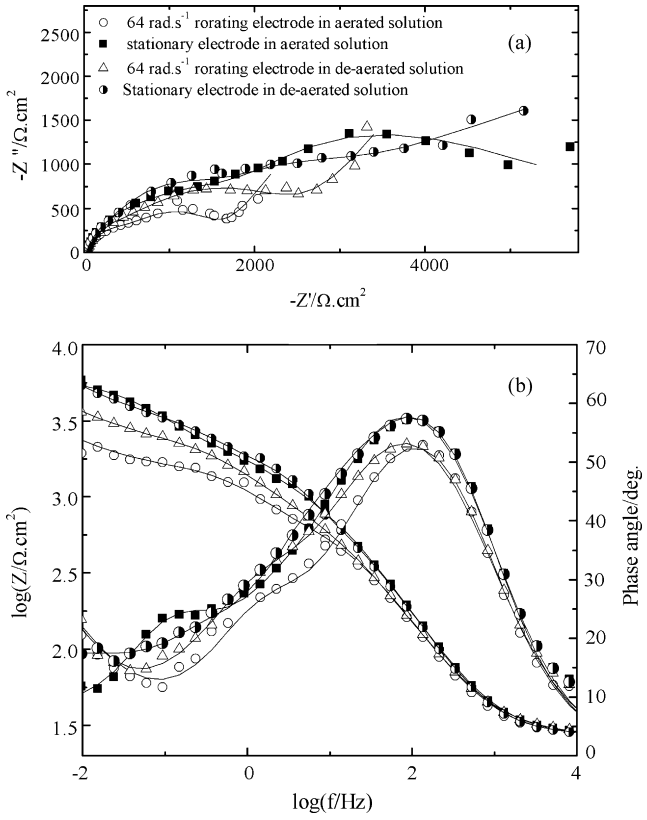

Fig. 8. Nyquist (a) and Bode (b) plots for the zinc electrode at −1200 mV in 0.1 M $KClO_4$ in the frquency range 10^4–10^{-2} Hz. Symbols represent the experimental data and solid lines represent the best fit.

the reduction of the dissolved O_2 and/or ClO_4^-, and a Warburg element, W, assigned to their diffusion towards the electrode surface. The fitting parameters are represented in Table 4. Plots of Fig. 7 show higher electrode impedance than those at −1.6 V (Fig. 5), referring to the beginning of the slow O_2 and/or ClO_4^- reduction. In addition, Nyquist plots of Fig. 7a exhibit a nearly ideal Warburg tail of a dihedral angle of 45° at low frequency range for the de-aerated. It tends to return to the real axis for naturally aerated solution.

In the potential range where the anodic dissolution of zinc takes place, the impedance spectra represented in Figs. 8 and 9 were obtained. Several models of equivalent circuits were attempted to fit these experimental data. The best agreement between experiment and fitting were obtained with the equivalent circuit of Fig. 6c. This circuit proposed the introduction of a third time constant to account for the simultaneous electrochemical reactions described in Section 3.3. It is evident that water reduction is doubtfully in this potential range. Moreover, it was stated that "under passivation conditions, a one step dissolution with activation and/or diffusion control is ascertained depending on the porosity of the corrosion layer" [6]. Therefore, the first time constant, $R_1 - Q_1$ circuit, may refer to the anodic zinc dissolution reaction. This circuit is conceived to include both of the corrosion layer resistance and the diffuse charge capacitance in the formed oxide layer [7]. The second, $WR_2 - Q_2$, assigned to O_2 and/or ClO_4^- reduction and their diffusion in the viscous part of the corrosion interphase. Furthermore, the third time constant

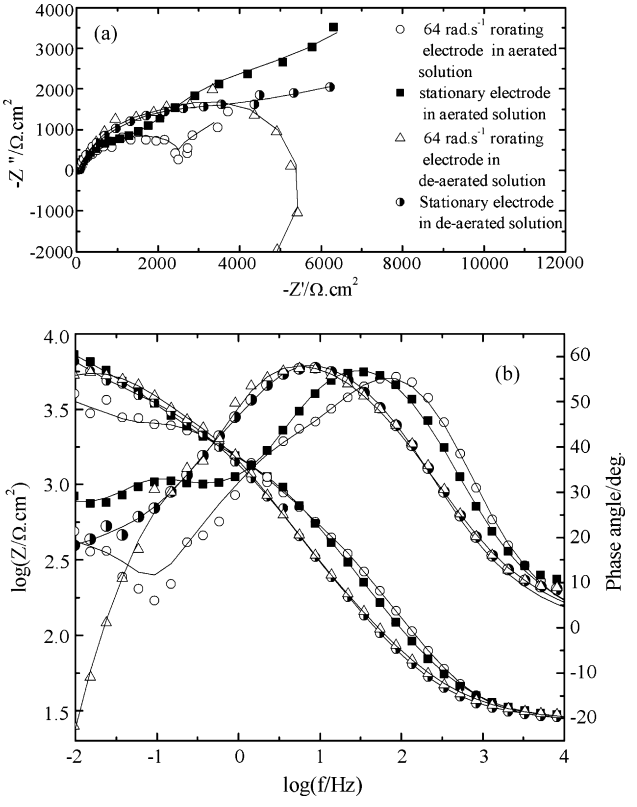

Fig. 9. Nyquist (a) and Bode (b) plots for the zinc electrode at −1100 mV in 0.1 M $KClO_4$ in the frquency range 10^4–10^{-2} Hz. Symbols represent the experimental data and solid lines represent the best fit.

Table 5
Impedance parameters obtained by fitting data of Figs. 8 and 9 with the equivalent circuit of Fig. 6c for the zinc electrode polarized at −1.2 and −1.1 V in 0.1 M $KClO_4$, respectively

Electrode potential (mV)	Solution	Electrode	Parameter										
			$R1$ (Ω)	$Q1$		$Q2$		$W \times 10^{-4}$	$R2$ (Ω)	$Q3$		$R3$ (Ω)	L (H)	$R4$ (Ω)
				Y (μF cm^{-2})	n	Y (μF cm^{-2})	n			Y (μF cm^{-2})	n			
−1200	Aerated	Stationary	1113	14.2	0.79	112.4	0.81	72.21	3400	4.3	0.81	934	1000	−216
		Rotating	1064	26.0	0.78	837.0	0.73	17.01	1768	3.9	0.80	524	163	−27
	De-aerated	Stationary	990	34.0	0.95	62.3	0.84	13.95	1901	3.9	0.80	2134	71570	−1695
		Rotating	1877	7.4	0.71	324.7	0.72	11.46	911	5.2	0.79	632	747	−142
−1100	Aerated	Stationary	3490	103.9	0.83	4.5	0.56	6.53	21150	10.2	0.82	110	1062	3490
		Rotating	2256	158.4	0.82	9.4	0.83	28.49	332	10.1	0.76	−82	2781	1431
	De-aerated	Stationary	2564	18.5	0.76	5.7	0.58		10420	430.3	1	851	10000	−662
		Rotating	1371	71.9	0.89	2.2	0.59		5180	2396	1	−6770	369100	7390

$R_o = 27$.

belonging probably to the cathodic Zn electrodeposition back reaction [6]. The induction element L (Fig. 6c) is introduced to account for the inductive loop that appear at very low frequency domain (Fig. 9). It may be correlated with the presence of the adsorbed intermediate species during the dissolution reaction [1,21] or the cathodic Zn electrodeposition back reaction [6]. It is suggested also to be related to the passive layer re-dissolution at low frequencies [38].

Macdonald [39] correlated the extent of the deviation from the ideal capacitive behaviour with the increase of the standard rate constant of the barrier layer dissolution. Likewise, the gradual decrease of $-S$ and α_{max} with electrode rotation and increasing potentials may be attributed to the higher passive layer dissolution rates (Figs. 7 and 8). The impedance of the electrode increases as potential shifts to more anodic values, because of the progressive passive film formation. However, it decreases when rotating the electrode confirming the formation of a less protective passive film in this condition (Table 5). On the other hand, the negative values of R_3 or R_4 give evidence for an inhibited passivation process as a result of the competition between the passive layer formation and its dissolution due to the induced basicity in the electrode vicinity [40,41,1].

4. Conclusions

The obtained results clarify the role of the dissolved O_2 in the formation of a more protective passive layer on the Zn anode surface in neutral solutions. The formed passive layer is suggested to be composed of interior compact thin layer formed by the O_2 chemisorption and an exterior porous $Zn(OH)_2$ /ZnO layer formed by a dissolution precipitation mechanism. Detection of Cl^- ion during the polarization of the Zn electrode at a wide range of potentials in perchlorate solutions confirms its reduction at the Zn surface with maximum rate at −1.4 V. De-aerating the perchlorate solution diminishes the interior passive layer formation probability. In addition, it leaves the chance for the adsorption of ClO_4^- ions on the electrode surface whose reduction to OH^- and Cl^- ions reduces the protection properties of the exterior passive layer formed in this condition as a result of enhancing its dissolution. The obtained impedance spectra confirm the evolution of the Zn/solution interphase with the applied potential. Depending on the applied potential, an equivalent circuits of one, two or three time constants were used to fit the experimental results. The decrease in the electrode impedance accompanying the electrode rotation validate the above conclusion concerning the formation of a less protective passive film in this condition.

References

[1] H.H. Hassan, Electrochim. Acta 51 (2006) 5966.
[2] H.H. Hassan, Appl. Surf. Sci. 174 (2001) 201.
[3] J. Swiatowska-Mrowiecka, J. Banaś, Electrochim. Acta 50 (2005) 1829.
[4] P. Kalinauskas, I. Valsiunas, M. Samuleviciene, E. Juzeliunas, Corros. Sci. 43 (2001) 2083.
[5] E.E. Foad El Sherbini, S.S. Abd El Rehim, Corros. Sci. 42 (2000) 785.
[6] L. Sziráki, E. Szöcs, Zs. Philbáth, K. Papp, E. Kálmán, Electrochim. Acta 46 (2001) 3743.

[7] L. Sziráki, A. Cziráki, I. Geröcs, Z. Vértesy, L. Kiss, Electrochim. Acta 43 (1998) 175.
[8] E.E. Abd El Aal, Corros. Sci. 44 (2002) 2041.
[9] C. Deslouis, M. Duprat, C. Tulet-Tournillon, J. Electroanal. Chem. 181 (1984) 119.
[10] Z. Nagy, D.A. Thomas, J. Electrochem. Soc. 133 (1986) 2013.
[11] A.A. El-Feki, G.W. Walter, Corros. Sci. 42 (2000) 1055.
[12] G. Láng, G. Inzelt, A. Vrabecz, G. Horányi, J. Electroanal. Chem. 582 (2005) 249 (and references therein).
[13] G. Láng, G. Horányi, J. Electroanal. Chem. 552 (2003) 197 (and references therein).
[14] M. Ujvári, G. Láng, G. Horányi, J. Appl. Electrochem. 31 (2001) 1171.
[15] M. Ujvári, G. Láng, G. Horányi, J. Appl. Electrochem. 32 (2002) 581.
[16] A.P. Yadav, A. Nishikata, T. Tsuru, J. Electroanal. Chem. 585 (2005) 142.
[17] L.M. Baugh, Electrochim. Acta 24 (1979) 657.
[18] http://www.efunda.com/materials/corrosion/electrochem_entry.cfm.
[19] C.M.V.B. Almeida, B.F. Giannetti, T. Rabockai, J. Electroanal. Chem. 422 (1997) 185.
[20] C. Cachet, R. Wiart, J. Electroanal. Chem. 129 (1981) 103.
[21] C. Cachet, F. Ganne, G. Maurin, J. Petitjean, V. Vivier, R. Wiart, Electrochim. Acta 47 (2001) 509.
[22] B.R. Strohmeier, D.M. Hercules, J. Catal. 86 (1984) 266.
[23] L.S. Dake, D.R. Bean, J.M. Zechara, Surf. Interface Anal. 14 (1989) 71.
[24] Z. Shuxian, W.K. Hall, G. Ertl, H. Knozinger, J. Catal. 100 (1986) 167.
[25] V.I. Nefedov, Y.V. Salyn, G. Leohardt, R. Scheibe, J. Electron Spectrosc. Relat. Phenom. 10 (1977) 121.
[26] M. Ayyoob, M.S. Hegde, J. Chem. Soc., Faraday Trans. 182 (1986) 1654.
[27] S. Gudić, J. Radošević, M. Kliškić, J. Appl. Electrochem. 26 (1996) 1027.
[28] S.Y. Zhao, S.H. Chen, H.Y. Ma, D.G. Li, F.J. Kong, J. Appl. Electrochem. 32 (2002) 231.
[29] H.Y. Ma, G.Q. Li, S.C. Chen, S.Y. Zhao, X.L. Cheng, Corros. Sci. 44 (2002) 1177.
[30] M.J. Justo, M.G.S. Ferreira, Corros. Sci. 34 (1993) 533.
[31] D. Giménez-Romero, J.J. García-Jareño, F. Vicente, J. Electroanal. Chem. 572 (2004) 235.
[32] J.R. Macdonald, W.B. Johanson, in: J.R. Macdonald (Ed.), Theory in Impedance Spectroscopy, J. Wiley & Sons, New York, 1987.
[33] W.A. Badawy, K.M. Ismail, A.M. Fathi, Electrochim. Acta 51 (2006) 4182.
[34] S.L.A. Maranh, I.C. Guedes, F.J. Anaissi, H.E. Tomac, I.V. Aoki, Electrochim. Acta 52 (2006) 519.
[35] P. Bommersbach, C. Alemany-Dumont, J.P. Millet, B. Normand, Electrochim. Acta 51 (2005) 1076.
[36] A.V. Benedetti, P.T.A. Sumodjo, K. Nobe, P.L. Cabot, W.G. Proud, Electrochim. Acta 40 (1995) 2657.
[37] B. Bartos, N. Hakerman, J. Electrochem. Soc. 139 (1992) 3428.
[38] E.M. Sherif, S.-M. Park, Electrochim. Acta 51 (2006) 1313.
[39] D.D. Macdonald, in: E. Barsoukov, J.R. Macdonald (Eds.), Impedance Spectroscopy, second ed., Wiley/Interscience, New York, 2005, p. 408.
[40] H.H. Hassan, Electrochim. Acta 51 (2005) 526.
[41] A.G. Muñoz, J.W. Schultze, Electrochim. Acta 49 (2004) 293.